

Cite this: *J. Mater. Chem. A*, 2024, 12, 13792Received 31st December 2023  
Accepted 5th February 2024

DOI: 10.1039/d3ta08126e

rsc.li/materials-a

# Photocatalytic oxidative cyclization of aromatic thioamides catalyzed by Cu<sub>2</sub>O rhombic dodecahedra†

Guan-Ru Wang and Michael H. Huang \*

Cu<sub>2</sub>O rhombic dodecahedra were used to photocatalyze thiobenzamide cyclization in tetrahydrofuran (THF) forming 3,5-diphenyl-1,2,4-thiadiazole under 390 nm light illumination. The rhombic dodecahedra outperform cubic and octahedral Cu<sub>2</sub>O crystals. They can also photocatalyze thiobenzamides bearing a wide range of substituent groups with generally high product yields in 18 h at room temperature. Electron, hole and various radical scavenging experiments were performed to support the proposed reaction mechanism. This work demonstrates again that the use of surface-controlled metal oxide crystals offers huge cost advantages over the covalent organic framework (COF) photocatalysts for some organic transformations.

## Introduction

Cu<sub>2</sub>O, Ag<sub>2</sub>O, Ag<sub>3</sub>PO<sub>4</sub>, SrTiO<sub>3</sub> and other polyhedral crystals have been shown to exhibit facet-dependent photocatalytic properties.<sup>1–6</sup> For instance, Cu<sub>2</sub>O rhombic dodecahedra are notably more photocatalytically active than octahedra, yet cubes are inert even with gold nanoparticle decoration.<sup>7</sup> Recent synchrotron X-ray diffraction (XRD) and high-resolution transmission electron microscopy (HR-TEM) characterization has revealed the presence of bulk and surface lattices in all Cu<sub>2</sub>O crystals, and different surfaces show distinct lattice deviation patterns.<sup>8</sup> Bulk cell constants also vary slightly for different particle shapes. Such structural feature should affect the barrier to charge transport across a particular crystal face, yielding the observed photocatalytic facet effect. Moreover, surface deposition of Cu<sub>2</sub>O polyhedra with various semiconductor nanocrystals including ZnO and ZnS can both enhance and suppress photocatalytic activity of the heterostructures depending on the interfacial planes with either favorable or unfavorable band bending.<sup>9,10</sup> Such interfacial contact selection is also useful to achieving current rectification.<sup>11</sup> Another way to boost photocatalytic activity is through surface conjugated molecular functionalization.<sup>12–14</sup> This is because surface band structure and electron density is greatly tuned with molecular modification.

Upon light illumination on semiconductor materials, the photoexcited electrons in the conduction band and holes in the valence band first migrate to the crystal surface. Electrons

reduce dissolved oxygen to form superoxide anion radicals (O<sub>2</sub><sup>•−</sup>), while holes oxidize water or hydroxide ions to give hydroxyl radicals (•OH).<sup>15,16</sup> Other than dye photodegradation and water splitting reactions, Cu<sub>2</sub>O crystals have been employed in CO<sub>2</sub> reduction.<sup>17–19</sup> The photogenerated charge carriers and radicals can also be utilized to catalyze some organic transformation reactions.<sup>20</sup> Previously, Cu<sub>2</sub>O rhombic dodecahedra have been demonstrated to efficiently photocatalyze arylboronic acid hydroxylation.<sup>21</sup> 4-Nitrophenylacetylene (4-NA)-modified Cu<sub>2</sub>O rhombic dodecahedra also photocatalyze aryl sulfide oxidation.<sup>22</sup> Oxidative amine coupling can also be performed using polyhedral SrTiO<sub>3</sub> and 4-NA-modified Cu<sub>2</sub>O crystals.<sup>23,24</sup> We further consider the formation of 1,2,4-thiadiazoles through photocatalytic thioamide cyclization reactions. 1,2,4-Thiadiazoles are an important class of heterocyclic compounds with biological and therapeutic applications ranging from anti-cancer to neuroprotective activity.<sup>25,26</sup> In the past, hypervalent-iodine(III)-mediated intramolecular oxidative reaction and CoPcS-catalyzed intramolecular reaction for the synthesis of 1,2,4-thiadiazole derivatives have been reported.<sup>27,28</sup> Iodine-mediated synthesis of 1,2,4-thiadiazoles is also known.<sup>29</sup> Organic oxidant has also been employed to form thioamides.<sup>30</sup> Use of Cu(OTf)<sub>2</sub> as a catalyst and K<sub>2</sub>CO<sub>3</sub> as a base in acetonitrile can also produce diverse thiobenzamides at 70 °C.<sup>31</sup> These procedures involve the use stoichiometric amounts of halogen as an oxidizing agent and base. More recently, covalent organic frameworks, such as fully conjugated Py-BSZ-COF containing an electron-donating unit and an electron-accepting unit, have been prepared at 120 °C for photocatalytic oxidative cyclization of diverse thioamides to 1,2,4-thiadiazoles or through photo-initiated intramolecular coupling.<sup>32–34</sup> Nevertheless, COFs are more complicated to synthesize and characterize. Making Py-BSZ-COF can take nearly 5 days.

Department of Chemistry, National Tsing Hua University, Hsinchu 300044, Taiwan.  
E-mail: hyhuang@mx.nthu.edu.tw

† Electronic supplementary information (ESI) available. See DOI: <https://doi.org/10.1039/d3ta08126e>



Here we demonstrate that simple Cu<sub>2</sub>O cubes, octahedra, and rhombic dodecahedra can photocatalyze thiobenzamide cyclization to form 3,5-diphenyl-1,2,4-thiadiazole. In particular, Cu<sub>2</sub>O rhombic dodecahedra show generally high conversion of diverse thioamides to 1,2,4-thiadiazoles in THF. Charge carrier and radical scavenging experiments were also performed to support the proposed reaction mechanism. This work further illustrates the great value of using surface-controlled semiconductor crystals for photocatalytic organic transformations.

## Results and discussion

### Characterization of Cu<sub>2</sub>O crystals

Cu<sub>2</sub>O cubes, rhombic dodecahedra, and octahedra were synthesized following our reported conditions.<sup>35</sup> Fig. 1 provides scanning electron microscopy (SEM) images of the synthesized Cu<sub>2</sub>O crystals, revealing high size and shape uniformity. Fig. S1, ESI† give their size distribution histograms. The average edge length of cubes is 307 nm. The average opposite corner length of octahedra is 292 nm, while the average opposite face length of

rhombic dodecahedra is 331 nm. XRD patterns of these samples, available in Fig. S2, ESI,† indicate exclusive formation of Cu<sub>2</sub>O. While cubes and octahedra have nearly identical peak positions, rhombic dodecahedra have peaks slightly shifted to lower 2θ angles from their larger cell constants. The results are consistent with synchrotron XRD measurements.<sup>8</sup> Such lattice constant variations give rise to their various facet-dependent behaviors.

For a fair comparison of the photocatalytic activity, the total particle surface area should be the same. With a fixed total surface area of 8.8 × 10<sup>15</sup> nm<sup>2</sup>, the amounts of Cu<sub>2</sub>O cubes, octahedra, and rhombic dodecahedra needed for the photocatalysis experiments are 2.7, 1.5 and 2.9 mg, respectively (Table S1, ESI†). A degassing and oxygen-filling process was carried out before adding thiobenzamide into a tube containing Cu<sub>2</sub>O rhombic dodecahedra to optimize the reaction conditions. Initially, solvent selection was examined (see Table 1). With the oxygen-filled glass tube, thiobenzamide conversion to 3,5-diphenyl-1,2,4-thiadiazole did not occur in water under 390 nm light-emitting diode (LED) light irradiation with a power of 40 W

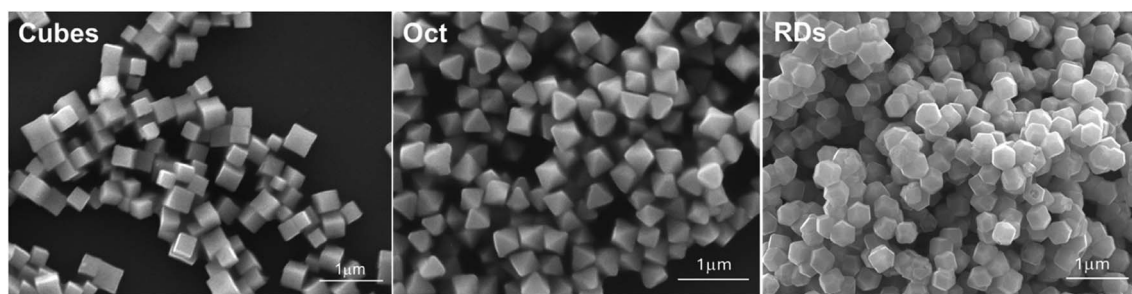
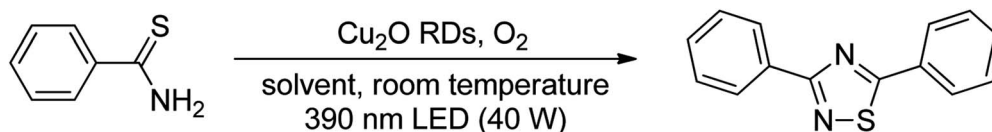


Fig. 1 SEM images of the synthesized Cu<sub>2</sub>O cubes, octahedra, and rhombic dodecahedra.

Table 1 Solvent effect on product yield<sup>a,b</sup>



Entry	Solvent	Time (h)	Yield (%)
1	Water	21	0
2	1,4-Dioxane	21	23
3	Toluene	21	31
4	Acetone	21	41
5	Ethyl acetate	21	52
6	Acetonitrile	21	58
7	Dichloromethane	21	63
8	Dichloroethane	21	69
9	Dimethylformamide	21	78
10	Ethanol	21	78
11	Methanol	21	80
12	Tetrahydrofuran	21	94

<sup>a</sup> Reagents: thiobenzamide (0.4 mmol), Cu<sub>2</sub>O RDs (2.9 mg) in solvent (3 mL). <sup>b</sup> Isolated yield.



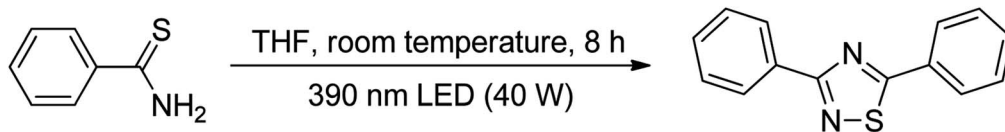
at room temperature. In 1,4-dioxane, toluene and acetone, the product yields reached to 23–41% after 21 h. Switching to ethyl acetate and acetonitrile, the yields improved to 52–58%. Use of dichloromethane and dichloroethane delivered yields of 63–69%. Further yield increases to 78–80% were observed in dimethylformamide, ethanol and methanol, so ethanol can be a good and green solvent choice for this reaction. However, the highest product yield of 94% was achieved using tetrahydrofuran as the solvent. Thus, tetrahydrofuran was chosen for subsequent optimization experiments.

The irradiation light wavelength effect was also examined (Table S2, ESI†). Use of 40 W 440 and 370 nm LED lamps gave product yields of 37 and 82%, respectively. With 390 nm light irradiation for 6 and 8 h, the product yields were 51 and 94%, respectively. Therefore, the 390 nm LED lamp remains most effective. Next, a series of control experiments for oxidative cyclization of thiobenzamide was conducted (Table 2). Use of commercial Cu<sub>2</sub>O powder only delivered 23% thiobenzamide conversion, showing the importance of catalyst surface control to reactivity. Without light irradiation, adding any catalyst, or introducing nitrogen, only a trace of amount of product was

obtained. This confirms that proper light illumination, catalyst and oxygen are all indispensable to achieving high product formation. Conducting the reaction in air atmosphere only gave 19% product yield, so filling the tube with oxygen is critically important. Additionally, when the reaction was carried out with the fan turned off, the solution temperature can reach 50 °C. The obtained product yield is 90%, so it is beneficial to use a fan to cool the solution.

Using the optimized reaction conditions, the product yield was 94% for {110}-bound Cu<sub>2</sub>O rhombic dodecahedra after 8 h of reaction as noted above (Table 3). By contrast, {100}-terminated cubes and {111}-enclosed octahedra showed 52 and 75% yields, respectively. Rhombic dodecahedra are clearly the best catalyst. This is understandable, since they are most efficient in charge transport to the surface for facile radical generation.<sup>7,36</sup> The notably high product yield in the case of Cu<sub>2</sub>O cubes should result from extended light irradiation to cause some degree of surface roughening. SEM images and XRD patterns of the particles taken after the photocatalysis reaction are provided in Fig. S3 and S4, ESI.† While octahedra and rhombic dodecahedra generally preserve their morphologies, some nanostructures

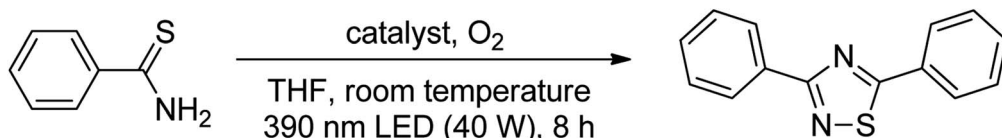
Table 2 Control experiments for oxidative cyclization of thioamide<sup>a,b</sup>



Entry	Catalyst	Light	O <sub>2</sub>	Yield (%)
1	+	+	+	94
2	+ <sup>c</sup>	+	+	23
3	–	+	+	Trace
4	+	–	+	Trace
5	+	+	– <sup>d</sup>	Trace
6	+	+	– <sup>e</sup>	19

<sup>a</sup> Reagents: thiobenzamide (0.4 mmol) and Cu<sub>2</sub>O RDs (2.9 mg) in THF (3 mL). <sup>b</sup> Isolated yield. <sup>c</sup> Commercially available Cu<sub>2</sub>O. <sup>d</sup> N<sub>2</sub> atmosphere. <sup>e</sup> Air atmosphere.

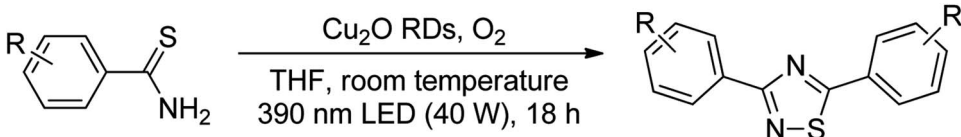
Table 3 Photocatalytic oxidative cyclization of thioamide using different Cu<sub>2</sub>O nanocrystals<sup>a,b</sup>

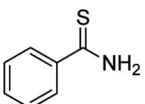
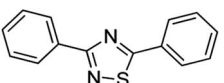
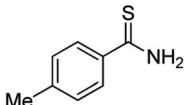
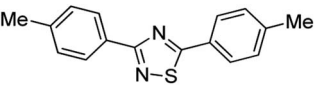
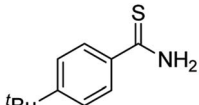
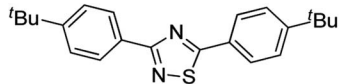
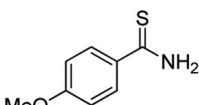
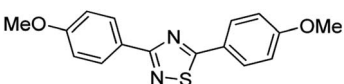
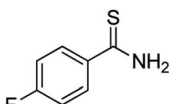
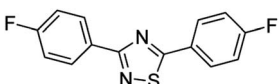
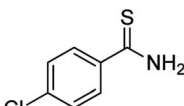
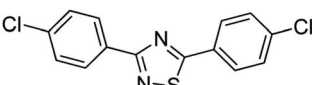
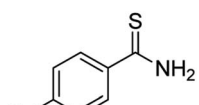
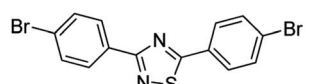
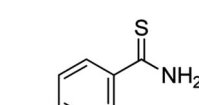
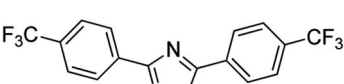
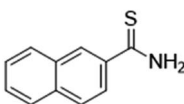
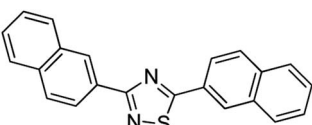
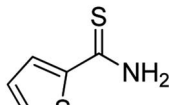
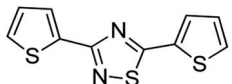
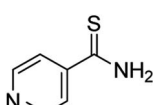
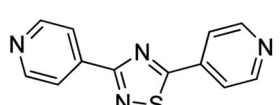


Entry	Catalyst	Amount (mg)	Yield (%)
1	Cu <sub>2</sub> O cubes	2.7	52
2	Cu <sub>2</sub> O octahedra	1.5	75
3	Cu <sub>2</sub> O rhombic dodecahedra	2.9	94

<sup>a</sup> Reagents: thiobenzamide (0.4 mmol) in THF (3 mL). <sup>b</sup> Isolated yield.



Table 4 Substrate scope of photocatalytic oxidative cyclization reactions<sup>a,b</sup>


Entry	Substrate	Product	Yield (%)
1 <sup>c</sup>			94
2			94
3			93
4			96
5			69
6			73
7			82
8			76
9			90
10			80
11			0

<sup>a</sup> Reagents: thioamide (0.4 mmol) and Cu<sub>2</sub>O RDs (2.9 mg) in THF (3 mL). <sup>b</sup> Isolated yield. <sup>c</sup> Time: 8 h.



appear on the cube surfaces. From X-ray photoelectron spectroscopy analysis, it has been observed before that continued light irradiation on Cu<sub>2</sub>O nanocubes can produce some CuO.<sup>36</sup> This surface change should make Cu<sub>2</sub>O cubes become photocatalytically active. XRD patterns of the used photocatalysts give only Cu<sub>2</sub>O diffraction peaks. Again rhombic dodecahedra possess a slightly larger cell constant than those of cubes and octahedra.

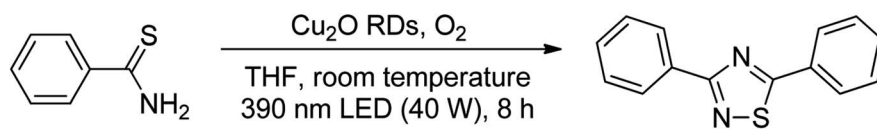
Substrate scope was examined next using the optimized reaction conditions with Cu<sub>2</sub>O rhombic dodecahedra as the photocatalyst. The reaction time was 18 h. Table 4 shows thio-benzamide bearing electron-donating 4-OCH<sub>3</sub>, 4-CH<sub>3</sub> and *tert*-butyl substituents can also achieve high product yields in the range of 93–96%. For the halogen-substituted thio-benzamides, generally good product yields of 69% (–F), 73% (–Cl), and 82% (–Br) were obtained. The results suggest that the electron-withdrawing ability of the halogen group is somewhat linked to the reactivity. For thio-benzamide with a highly electronegative trifluoromethyl group, a product yield of 76% was obtained. Furthermore, use of a naphthalene-substituted thioamide for oxidative coupling resulted in 90% product yield. Last, use of a heterocyclic thiophene-substituted thioamide gave a product yield of 80%, but the pyridinyl-substituted thioamide showed no product formation. A lack of reactivity for pyridinylboronic acid hydroxylation has been observed before.<sup>21</sup> Despite the pyridinyl inactivity, these experiments demonstrate that Cu<sub>2</sub>O rhombic dodecahedra are capable of photocatalyzing cyclization reaction of a diverse range of thioamides.

To propose a reaction mechanism, electron, hole, and radical scavenging experiments need to be performed first using the optimized reaction conditions with Cu<sub>2</sub>O rhombic dodecahedra as the photocatalyst. As seen in Table 5, adding potassium persulfate (K<sub>2</sub>S<sub>2</sub>O<sub>8</sub>) as an electron scavenger led to a significant drop in thio-benzamide conversion to just 21%.<sup>37</sup> This infers that the photoexcited electrons are utilized to generate radicals for thioamide cyclization. When KI was introduced as a hole scavenger, 3,5-diphenyl-1,2,4-thiadiazole formation was reduced to 11%. Employing sodium oxalate as another hole scavenger, a trace

amount of product formation was recorded. Thus, holes should participate in the photoredox reaction to facilitate thioamide cyclization. Next, addition of 1,4-benzoquinone to the reaction solution to remove superoxide anion radicals led to a significant product decrease to just 27%, indicating the active role of superoxide radicals to product formation. Previous electron paramagnetic resonance (EPR) measurements on photoirradiated Cu<sub>2</sub>O rhombic dodecahedra dispersed in methanol also revealed the formation of superoxide anion radicals.<sup>21,22</sup> Introducing DABCO as singlet oxygen scavenger reduces the product yield to 32%. Singlet oxygen molecules have been suggested to involve in photocatalytic benzylamine coupling reactions.<sup>23</sup> Singlet oxygen is produced upon photoexcitation of the ground state triplet oxygen. It is subsequently reduced to form a superoxide anion radical. Removal of singlet oxygen molecules lowers the production of superoxide radicals. Last, adding isopropanol as a hydroxyl radical scavenger had a relatively minor effect with a product yield of 82%, so hydroxyl radicals are less important in the photocatalytic process. The above results are consistent with the band positions of these Cu<sub>2</sub>O crystals. With their conduction band energies at around –1.40 V vs. RHE (reversible hydrogen electrode), oxygen reduction to form superoxide radicals at a standard potential of –0.33 V should happen.<sup>38</sup> However, their valence band positions at around 0.70 V is not capable of carrying out direct water oxidation to yield hydroxyl radicals (2.73 V).<sup>39</sup> An alternative pathway *via* water oxidation to molecular oxygen first (1.23 V), followed by the formation of H<sub>2</sub>O<sub>2</sub> at 0.68 V, is more reasonable.<sup>40</sup> Subsequent hydrogen peroxide reduction, photolysis, or reaction with superoxide radicals, gives hydroxyl radicals. Water oxidation by Cu<sub>2</sub>O is possible, considering surface band bending should exist to explain the observed facet-dependent behaviors.

From the above results, along with related literature reports, a plausible mechanism of the photocatalytic oxidative cyclization reaction is proposed, as illustrated in Fig. 2.<sup>32,34</sup> Under light irradiation, electron-hole pairs are generated within Cu<sub>2</sub>O rhombic dodecahedra and then migrate to the surface. The photogenerated holes participate in the oxidation of thioamide

Table 5 Reactive oxygen species, electron and hole trapping experiments<sup>a,b</sup>



Entry	Trapping reagent	Yield (%)
1 <sup>c</sup>	K <sub>2</sub> S <sub>2</sub> O <sub>8</sub>	21
2 <sup>d</sup>	KI	11
3 <sup>d</sup>	Sodium oxalate	Trace
4 <sup>e</sup>	1,4-Benzoquinone	27
5 <sup>f</sup>	DABCO	32
6 <sup>g</sup>	Isopropanol	82

<sup>a</sup> Reagents: thio-benzamide (0.4 mmol) and Cu<sub>2</sub>O RDs (2.9 mg) in THF (3 mL). <sup>b</sup> Isolated yield. <sup>c</sup> K<sub>2</sub>S<sub>2</sub>O<sub>8</sub> as electron scavenger. <sup>d</sup> KI and sodium oxalate as hole scavengers. <sup>e</sup> 1,4-Benzoquinone as O<sub>2</sub><sup>•-</sup> radical scavenger. <sup>f</sup> DABCO as <sup>1</sup>O<sub>2</sub> scavenger. <sup>g</sup> Isopropanol as <sup>•</sup>OH scavenger.





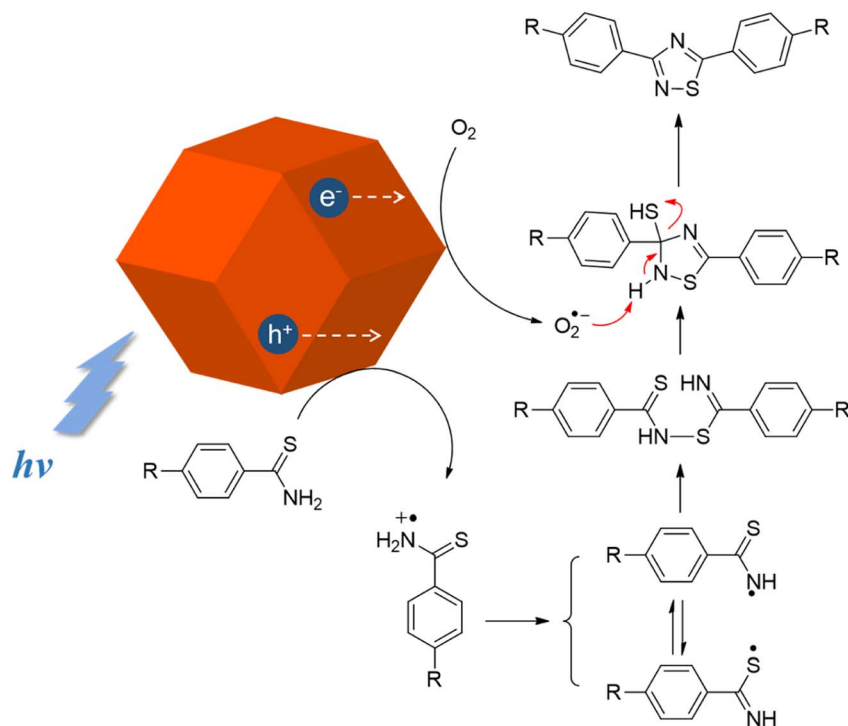


Fig. 2 Proposed reaction mechanism of  $\text{Cu}_2\text{O}$ -catalyzed photocatalytic oxidative cyclization reaction of thioamides.

and convert the molecules into corresponding cationic radicals. The thioamide radical cations first transform into two radical isomers after proton removal, which are linked to give a dimer through radical cross-coupling. The photogenerated electrons would reduce oxygen to form superoxide radicals. Through proton abstraction by superoxide radicals, 1,2,4-thiadiazole is readily obtained *via* intramolecular cyclization of the dimer and subsequent aromatization with removal of  $\text{SH}^-$  species.

## Conclusions

$\text{Cu}_2\text{O}$  rhombic dodecahedra were used to optimize the reaction conditions toward photocatalytic oxidative cyclization of thio-benzamide. Under the optimized reaction conditions, rhombic dodecahedra can achieve 94% product yield with 390 nm LED illumination in just 8 h, while cubes and octahedra delivered lower product yields.  $\text{Cu}_2\text{O}$  rhombic dodecahedra can also photocatalyze thiobenzamides bearing a broad range of substituent groups with generally high product yields. Charge carrier and radical scavenging experiments were conducted to support a plausible reaction mechanism. The use of polyhedral cuprous oxide crystals for this organic transformation offers tremendous cost advantages over COF photocatalysts.

## Experimental

### Chemicals

Sodium dodecyl sulfate (SDS, 100%, J. T. Baker), anhydrous copper(II) chloride ( $\text{CuCl}_2$ , 98%, Alfa Aesar), sodium hydroxide (NaOH, 98%, SHOWA), hydroxylamine hydrochloride

( $\text{NH}_2\text{OH}\cdot\text{HCl}$ , 99%, Alfa Aesar), potassium carbonate ( $\text{K}_2\text{CO}_3$ , 99%, Alfa Aesar), acetone ( $\text{C}_3\text{H}_6\text{O}$ , 97%, Alfa Aesar), acetonitrile ( $\text{CH}_3\text{CN}$ , 99%, Alfa Aesar), dichloroethane ( $\text{C}_2\text{H}_4\text{Cl}_2$ , 99.8%, Sigma-Aldrich), dichloromethane ( $\text{CH}_2\text{Cl}_2$ , >95%, Alfa Aesar), *N,N*-dimethylmethanamide ( $\text{C}_3\text{H}_7\text{NO}$ , 99%, Alfa Aesar), 1,4-dioxane ( $\text{C}_4\text{H}_8\text{O}_2$ , 99.8%, Sigma-Aldrich), ethanol ( $\text{C}_2\text{H}_5\text{OH}$ ,  $\geq 99.5\%$ , Honeywell), ethyl acetate ( $\text{C}_4\text{H}_8\text{O}_2$ , >99.5%, Alfa Aesar), *n*-hexane ( $\text{C}_6\text{H}_{14}$ ,  $\geq 95\%$ , Sigma-Aldrich), methanol ( $\text{CH}_3\text{OH}$ ,  $\geq 99.8\%$ , Honeywell), tetrahydrofuran ( $\text{C}_4\text{H}_8\text{O}$ , THF,  $\geq 99.9\%$ , Sigma-Aldrich), toluene ( $\text{C}_6\text{H}_5\text{CH}_3$ , 99.5%, Alfa Aesar), DABCO ( $\text{C}_6\text{H}_{12}\text{N}_2$ , >99%, Sigma-Aldrich), 1,4-benzoquinone ( $\text{C}_6\text{H}_4\text{O}_2$ , 98%, Alfa Aesar), potassium persulfate ( $\text{K}_2\text{S}_2\text{O}_8$ ,  $\geq 99.0\%$ , Sigma-Aldrich), potassium iodide (KI, 99.5%, J. T. Baker), sodium oxalate ( $\text{Na}_2\text{C}_2\text{O}_4$ ,  $\geq 99.0\%$ , Sigma-Aldrich), isopropanol ( $\text{C}_3\text{H}_8\text{O}$ , 99.5%, Sigma-Aldrich), thiobenzamide ( $\text{C}_6\text{H}_5\text{CSNH}_2$ , 98%, Sigma-Aldrich), 4-methylbenzothioamide ( $\text{C}_8\text{H}_9\text{NS}$ , >98.0%, TCI), 4-methoxythiobenzamide ( $\text{C}_8\text{H}_9\text{NOS}$ , 98%, Alfa Aesar), 4-*tert*-butylthiobenzamide ( $\text{C}_{11}\text{H}_{15}\text{NS}$ , 98%, Sigma-Aldrich), 4-fluorothiobenzamide ( $\text{C}_7\text{H}_6\text{FNS}$ , 97%, Alfa Aesar), 4-chlorothiobenzamide ( $\text{C}_7\text{H}_6\text{ClNS}$ , 97%, TCI), 4-bromothiobenzamide ( $\text{C}_7\text{H}_6\text{BrNS}$ , 97%, Thermo), 4-(trifluoromethyl)thiobenzamide ( $\text{C}_8\text{H}_6\text{F}_3\text{NS}$ , 98%, TCI), naphthalene-2-thiocarboxamide ( $\text{C}_{11}\text{H}_9\text{NS}$ , 97%, Thermo), thiophene-2-carbothioamide ( $\text{C}_5\text{H}_5\text{NS}_2$ , 99%, TCI), and 4-pyridinethioamide ( $\text{C}_6\text{H}_6\text{N}_2\text{S}$ , 97%, Sigma-Aldrich) were used as received. All the water (18.2 M $\Omega$ ) used was purified by the Milli-Q technique.

### $\text{Cu}_2\text{O}$ -photocatalyzed oxidative cyclization of thioamides

Synthesis conditions of  $\text{Cu}_2\text{O}$  cubes, octahedra, and rhombic dodecahedra are provided in the ESI.† Also see Fig. S5, ESI† for



an illustration of the crystal synthesis procedure. Typically, rhombic dodecahedral Cu<sub>2</sub>O crystals (2.9 mg) and thioamide (0.4 mmol) were added to a 15 mL quartz test tube with a stir bar and sealed with a rubber septum. The tube was evacuated using a vacuum pump and refilled with oxygen three times. After the evacuation and refill steps, tetrahydrofuran was injected into the tube. The mixture was sonicated for 3 min and placed approximately 2 cm from a blue LED lamp (40 W,  $\lambda = 390$  nm). See Fig. S6, ESI† for the sample preparation illustration. The photocatalytic reaction was carried out for 8 h with the aid of a cooling fan to maintain the solution temperature near room temperature. Cu<sub>2</sub>O crystals were separated by centrifugation at 10 000 rpm for 3 min. The separated organic layer was concentrated by rotary evaporation to obtain the crude product. The residue was purified by short column chromatography.

### Instrumentation

SEM images of the samples were obtained using a JOEL JSM-7000F electron microscope. XRD patterns were collected using a D2 PHASER desktop diffractometer with Cu K $\alpha$  radiation ( $\lambda = 0.1541$  Å). UV-Vis absorption spectra were taken with the use of a JASCO V-770 spectrophotometer. A Kessil KSPR160-L lamp was used in the photocatalytic experiments. <sup>1</sup>H and <sup>13</sup>C NMR spectra were recorded on a Bruker Avance 400 spectrometer. Chemical shifts ( $\delta$ ) are reported in ppm with the residual solvent signal as internal standard (chloroform at 7.26 and 77.00 ppm for <sup>1</sup>H and <sup>13</sup>C NMR spectroscopy, respectively). Thin-layer chromatography (TLC) was conducted on silica-gel 60 F254 plates (Merck KGaA).

### Conflicts of interest

There are no conflicts to declare.

### Acknowledgements

Financial support is provided by the National Science and Technology Council, Taiwan (NSTC 112-2113-M-007-016-MY3).

### References

- M. H. Huang and M. Madasu, *Nano Today*, 2019, **28**, 100768.
- Y.-J. Chen, Y.-W. Chiang and M. H. Huang, *ACS Appl. Mater. Interfaces*, 2016, **8**, 19672–19679.
- Y.-W. Harn, T.-H. Yang, T.-Y. Tang, M.-C. Chen and J.-M. Wu, *ChemCatChem*, 2015, **7**, 80–86.
- D. Majumder, I. Chakraborty, K. Mandal and S. Roy, *ACS Omega*, 2019, **4**, 4243–4251.
- M.-S. Hsieh, H.-J. Su, P.-L. Hsieh, Y.-W. Chiang and M. H. Huang, *ACS Appl. Mater. Interfaces*, 2017, **9**, 39086–39093.
- P.-L. Hsieh, G. Naresh, Y.-S. Huang, C.-W. Tsao, Y.-J. Hsu, L.-J. Chen and M. H. Huang, *J. Phys. Chem. C*, 2019, **123**, 13664–13671.
- C.-Y. Chu and M. H. Huang, *J. Mater. Chem. A*, 2017, **5**, 15116–15123.
- B.-H. Chen, G. Kumar, Y.-J. Wei, H.-H. Ma, J.-C. Kao, P.-J. Chou, Y.-C. Chuang, I.-C. Chen, J.-P. Chou, Y.-C. Lo and M. H. Huang, *Small*, 2023, **19**, 2303491.
- S.-C. Wu, C.-S. Tan and M. H. Huang, *Adv. Funct. Mater.*, 2017, **27**, 1604635.
- G. Naresh, P.-L. Hsieh, V. Meena, S.-K. Lee, Y.-H. Chiu, M. Madasu, A.-T. Lee, H.-Y. Tsai, T.-H. Lai, Y.-J. Hsu, Y.-C. Lo and M. H. Huang, *ACS Appl. Mater. Interfaces*, 2019, **11**, 3582–3589.
- A.-T. Lee, C.-S. Tan and M. H. Huang, *ACS Cent. Sci.*, 2021, **7**, 1929–1937.
- S.-J. Chan, J.-C. Kao, P.-J. Chou, Y.-C. Lo, J.-P. Chou and M. H. Huang, *J. Mater. Chem. C*, 2022, **10**, 8422–8431.
- A. S. Patra, J.-C. Kao, S.-J. Chan, P.-J. Chou, J.-P. Chou, Y.-C. Lo and M. H. Huang, *J. Mater. Chem. C*, 2022, **10**, 3980–3989.
- P.-J. Chou, W.-Y. Yu, J.-C. Kao, Y.-C. Lo, J.-P. Chou and M. H. Huang, *J. Mater. Chem. A*, 2023, **11**, 19514–19523.
- D. Nunes, A. Pimental, R. Branquinho, E. Fortunato and R. Martins, *Catalysts*, 2021, **11**, 504.
- Y.-H. Zhang, M.-M. Liu, J.-L. Chen, S.-M. Fang and P.-P. Zhou, *Dalton Trans.*, 2021, **50**, 4091–4111.
- T. Zhu, B. Wu, J. Xie, H. Yang, W. Zhang and Y. Sun, *ACS Sustainable Chem. Eng.*, 2023, **11**, 17482–17491.
- J. Lu, L. Yang, Y. Zhang, C. Wang, C. Zhang and X. S. Zhao, *ACS Appl. Nano Mater.*, 2023, **6**, 20746–20756.
- C.-f. Li, R.-t. Guo, Z.-r. Zhang, T. Wu and W.-g. Pan, *Small*, 2023, **19**, 2207875.
- S. Rej, M. Bisetto, A. Naldoni and P. Fornasiero, *J. Mater. Chem. A*, 2021, **9**, 5915–5951.
- Z.-H. Su, M.-H. Hsieh, Z.-L. Chen, W.-T. Dai, E.-T. Wu and M. H. Huang, *Chem. Mater.*, 2023, **35**, 2782–2789.
- M.-H. Hsieh, Z.-H. Su, E.-T. Wu and M. H. Huang, *ACS Appl. Mater. Interfaces*, 2023, **15**, 11662–11669.
- Z.-L. Chen and M. H. Huang, *J. Mater. Chem. A*, 2023, **11**, 22198–22205.
- E.-T. Wu and M. H. Huang, *ACS Catal.*, 2023, **13**, 14746–14752.
- Y. J. Pragathi, R. Screenivasulu, D. Veronica and R. R. Raju, *Arabian J. Sci. Eng.*, 2021, **46**, 225–232.
- G. L. Perlovich, A. N. Proshin, T. V. Volkova, L. N. Petrova and S. O. Bachurin, *Mol. Pharm.*, 2012, **9**, 2156–2167.
- A. Mariappan, K. Rajaguru, N. M. Chola, S. Muthusubramanian and N. Bhuvanesh, *J. Org. Chem.*, 2016, **81**, 6573–6579.
- L. Yang, L. Song, S. Tang, L. Li, H. Li, B. Yuan and G. Yang, *Eur. J. Org. Chem.*, 2019, 1281–1285.
- N. Jatangi, N. Tumula, R. K. Palakodety and M. Nakka, *J. Org. Chem.*, 2018, **83**, 5715–5723.
- D. Cheng, R. Luo, W. Zheng and J. Yan, *Synth. Commun.*, 2012, **42**, 2007–2013.
- Y. Sun, W. Wu and H. Jiang, *Eur. J. Inorg. Chem.*, 2014, 4239–4243.
- S. Li, L. Li, Y. Li, L. Dai, C. Liu, Y. Liu, J. Li, J. Lv, P. Li and B. Wang, *ACS Catal.*, 2020, **10**, 8717–8726.
- J. Yuan, Q. Xia, W. Zhu, C. Wu, B. Wang, B. Liu, X. Yang, Y. Xu and H. Xu, *ChemPhotoChem*, 2020, **4**, 445–450.



- 34 Y. Liu, X. Jiang, L. Chen, Y. Cui, Q.-Y. Li, X. Zhao, X. Han, Y.-C. Zheng and X.-J. Wang, *J. Mater. Chem. A*, 2023, **11**, 1208–1215.
- 35 H.-H. Ma and M. H. Huang, *J. Mater. Chem. C*, 2023, **11**, 5857–5866.
- 36 G.-Z. Yuan, C.-F. Hsia, Z.-W. Lin, C. Chiang, Y.-W. Chiang and M. H. Huang, *Chem.–Eur. J.*, 2016, **22**, 12548–12556.
- 37 M.-Q. Yang, C. Han, N. Zhang and Y.-J. Xu, *Nanoscale*, 2015, **7**, 18062–18070.
- 38 P. Ren, T. Zhang, N. Jain, H. Y. V. Ching, A. Jaworski, G. Barcaro, S. Monti, J. Silvestre-Albero, V. Celorrio, L. Chouhan, A. Rokicińska, E. Debroye, P. Kuśtrowski, S. Van Doorslaer, S. Van Aert, S. Bals and S. Das, *J. Am. Chem. Soc.*, 2023, **145**, 16584–16596.
- 39 S. Siahrostami, G.-L. Li, V. Viswanathan and J. K. Nørskov, *J. Phys. Chem. Lett.*, 2017, **8**, 1157–1160.
- 40 S. Wu and X. Quan, *ACS ES&T Engg.*, 2022, **2**, 1068–1079.

